CONTROL OF PARALLEL MANIPULATORS USING FORCE FEEDBACK

Prabjot Nanua
University of Houston
Houston, Texas

Abstract

Parallel robotic mechanisms have good accuracy, high stiffness and large payload to weight ratio compared to the traditional serial mechanism. This paper compares two simple constant gain control schemes for a parallel robotic mechanism actuated by hydraulic cylinders. One of the control schemes which will be referred to as a "rate based scheme" uses the position and rate information only for feedback. The other control scheme referred to as the "force based scheme" feeds back the force information also. It is shown that for parallel robots with hydraulic actuators the response of the end-effector can be improved by using the force information from the actuators without adding any extra computational burden. The force based control scheme can also be easily modified to control the forces on the end-effector. The control scheme has been implemented in a computer simulation and the results are presented in the paper.

Introduction

Recently, there has been a lot of activity in the area of parallel mechanisms (Figure 1). Parallel mechanisms are able to overcome many of the shortcomings of serial mechanisms. They have a high stiffness, large payload to weight ratio and good accuracy compared to serial mechanisms. The best known application of parallel mechanism is the Stewart Platform which is used in aircraft simulators. These mechanisms also have potential for application in zero/partial gravity simulators, assembly tasks and precision machining.

Previous research in parallel mechanisms has been focused on the kinematics of the mechanisms. The general kinematic considerations are examined in [3], [4], [7], [13] and [14]. The direct position kinematics of some special parallel mechanisms are given in [5], [9] and [10]. There is little research in the dynamics and controls of parallel mechanisms. Some of the dynamics issues are examined in [15].

An important part of assembly tasks is the control of interaction forces between components. In other applications such as partial/zero gravity simulators, it will be required that the actuators apply constant forces through the center of mass of the end effector. In this application, again the forces on the end effector will have to be controlled. The rate based scheme does not offer any capability for controlling forces. The force based control scheme developed in this paper can easily be modified to control these forces. This ability is crucial to the successful application of parallel mechanisms to assembly tasks.

The parallel mechanism analyzed in this paper is shown in Figure 1. It is a six degree of freedom mechanism. The top member and the base member are connected by six limbs. Each limb is a hydraulic cylinder with universal joints at each end. The piston and the cylinder are allowed to rotate with respect to each other. Thus each limb is a six degree of freedom serial chain with one actuated prismatic joint. The universal joints in the top member are located in a plane and the universal joints in the base member are also located in a single plane.

The first section of the paper examines the linearized dynamic model of the fully parallel mechanism. Using the linearized model, the control schemes are studied. The following section describes the control scheme in detail. The next section deals with the

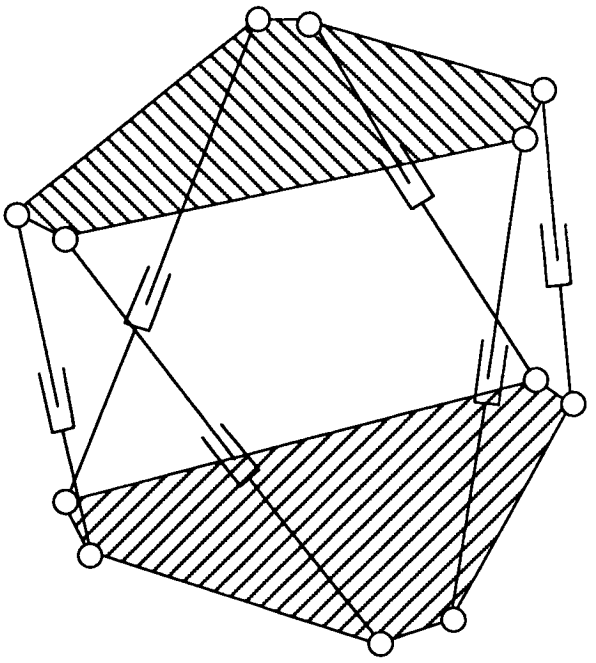

Figure 1. Special Parallel Mechanism (Each limb consists of universal joints at each end and a cylinderical joint between them; the prismatic joint is actuated).

complete dynamic simulation of the parallel mechanism. To simulate the dynamics of the mechanism, it is essential to have an efficient scheme for the direct dynamics problem. This will help in reducing the computational time required for simulation. The models for the hydraulic cylinders and the servolvalves are given in Appendix B. The results are discussed in the last section.

Linearized Rigid Body Model

In fully parallel mechanisms ([14]), the joint rates and the end effector motion are related by the following equation:

$$\dot{\mathbf{L}} = \mathbf{H}^{\mathrm{T}} \begin{bmatrix} \omega \\ \mu \end{bmatrix} \tag{1}$$

where
$\dot{\mathbf{L}}$ = Vector consisting of the joint rates.
$\mathbf{H}$ = 6×6 matrix.
ω = angular velocity of the end effector.
μ = velocity of the point on the end effector coincident with the origin.

The matrix $\mathbf{H}$ is a purely geometric quantity. The columns of the matrix $\mathbf{H}$ are the wrench axis of the joints.

For parallel mechanisms, static force decomposition equation is:

$$\begin{bmatrix} \mathbf{R} \\ \Gamma \end{bmatrix} = \mathbf{HF} \tag{2}$$

where
$\mathbf{R}$ = Forces acting on the end effector.
Γ = Moments acting on the end effector about the origin.
$\mathbf{H}$ = 6×6 matrix
$\mathbf{F}$ = Forces/Torque's at the joints.

It will be assumed without any loss of generality that the origin of the fixed coordinate system is located at the nominal position of the center of mass of the end-effector.

The current approach, based on the rate control scheme, is to control the joint lengths in the parallel mechanism. Using this scheme, current position of the end effector is compared to the desired position. The error in the position is converted to an error in the length of the limbs. The limbs are then individually controlled to eliminate this error. This is achieved by applying forces in the limbs that are proportional to the error in the limb lengths. This is given by the equation:

$$\mathbf{F} = -\mathbf{K}_p\mathbf{L} - \mathbf{K}_v\dot{\mathbf{L}} \tag{3}$$

where
$\mathbf{L}$ = error in the limb lengths.

The equation of motion of the end effector is given by (ignoring the non-linear terms):

$$\begin{bmatrix} \mathbf{M} & \mathbf{0} \\ \mathbf{0} & \mathbf{J} \end{bmatrix} \begin{bmatrix} \ddot{\mathbf{p}} \\ \ddot{\theta} \end{bmatrix} = \begin{bmatrix} \mathbf{R} \\ \Gamma \end{bmatrix} \tag{4}$$

where
$\mathbf{M}$ = Diagonal matrix with the mass of the end effector as the diagonal term.
$\mathbf{J}$ = Moment of inertia matrix at the current position.
$\mathbf{p}, \theta$ = small errors in position and orientation of end effector.

Using equations (2), (3) and (4), the response equation is (ignoring the actuator model):

$$\begin{bmatrix} \mathbf{M} & \mathbf{0} \\ \mathbf{0} & \mathbf{J} \end{bmatrix} \begin{bmatrix} \ddot{\mathbf{p}} \\ \ddot{\theta} \end{bmatrix} + \mathbf{H}\mathbf{K}_v\mathbf{H}^{\mathrm{T}} \begin{bmatrix} \dot{\mathbf{p}} \\ \dot{\theta} \end{bmatrix} + \mathbf{H}\mathbf{K}_p\mathbf{H}^{\mathrm{T}} \begin{bmatrix} \mathbf{p} \\ \theta \end{bmatrix} = \mathbf{0} \tag{5}$$

The gain matrices in the above equation, $\mathbf{K}_p$ and $\mathbf{K}_v$ are diagonal matrices with constant terms (the cylinders are controlled independently with constant gains). Clearly, the response depends on the matrix $\mathbf{H}$, which depends on the position of the end effector. This is undesirable. It is also not obvious from the above equation, whether an increase in the gains would lead to an improvement in the response of the mechanism. Increase in the gains might lead to deterioration in the response due to the structure of the $\mathbf{H}$ matrix. Further, increasing the gains, leads to a shift in all the closed loop poles of the above system. The fast poles as well as the slow poles are moved simultaneously. This leads to a marginal improvement in the response of the system with large changes in the gains. There is also the possibility of exciting the higher order dynamics due to the presence of fast poles (as a result of increase in gains).

As opposed to the above rate based scheme, in the force based control scheme, the force is controlled in each limb. The error in the current position of the end effector is fed back as error in the forces exerted by the limbs. This is given by the equation:

$$\begin{bmatrix} \mathbf{R} \\ \Gamma \end{bmatrix} = -\mathbf{K}_p \begin{bmatrix} \mathbf{p} \\ \theta \end{bmatrix} - \mathbf{K}_v \begin{bmatrix} \dot{\mathbf{p}} \\ \dot{\theta} \end{bmatrix} \tag{6}$$

The force to be produced by the actuators at the limbs is given by (equation (2) and (6)):

$$\mathbf{F} = -\mathbf{H}^{-1}\left(\mathbf{K}_p\begin{bmatrix}\mathbf{p}\\ \theta\end{bmatrix} + \mathbf{K}_v\begin{bmatrix}\dot{\mathbf{p}}\\ \dot{\theta}\end{bmatrix}\right) \tag{7}$$

The response equation is now given by (combining equations (4) and (6)):

$$\begin{bmatrix}\mathbf{M} & \mathbf{0}\\ \mathbf{0} & \mathbf{J}\end{bmatrix}\begin{bmatrix}\ddot{\mathbf{p}}\\ \ddot{\theta}\end{bmatrix} + \mathbf{K}_v\begin{bmatrix}\dot{\mathbf{p}}\\ \dot{\theta}\end{bmatrix} + \mathbf{K}_p\begin{bmatrix}\mathbf{p}\\ \theta\end{bmatrix} = \mathbf{0} \tag{8}$$

In a simple implementation of the above scheme, $\mathbf{K}_p$ and $\mathbf{K}_v$ can be chosen as diagonal matrices with fixed diagonal terms. The response equations are now to a large extent position independent and decoupled. The response does not depend on the **H** matrix. The coupling and the position dependency in the above equation will come from the **J** matrix. This response equation is an improvement over the previous scheme. The closed loop poles can be assigned independently in the above scheme and the response improved without a corresponding large increase in the gains.

The above scheme can also be easily adapted to control the forces on the end effector. The direction in which forces are to be controlled can easily replace the position errors in equation (6). This would effectively control the forces in those directions.

Dynamic Simulation and Control Scheme of the Parallel Mechanism

A rigid body dynamic model was developed for the parallel mechanism for simulation in MATRIXX. Some of the assumptions made for the dynamic model are as follows. The limbs were assumed to be axisymmetric. The friction losses in the spherical and revolute joints were assumed to be negligible. The prismatic joint in the cylinder was assumed to have viscous losses and the damping coefficient was adjusted to obtain a response that closely approximated the response from the actual mechanism. The model for the hydraulic cylinders consists of a leakage term which is assumed to be proportional to the pressure difference in the cylinder (assuming that the leakage flow is laminar). The model for the servovalves was taken from [8].

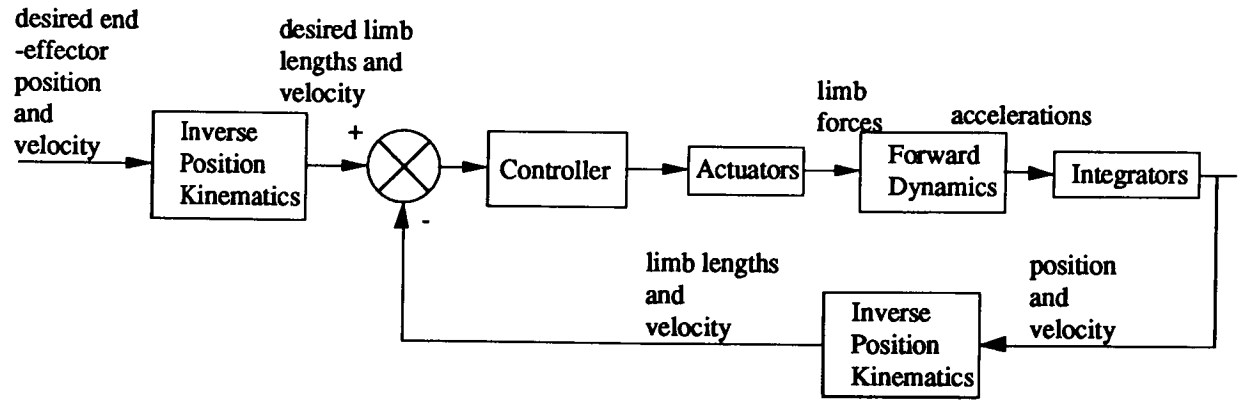

Figure 2. Block Diagram for Rate Based Control Scheme.

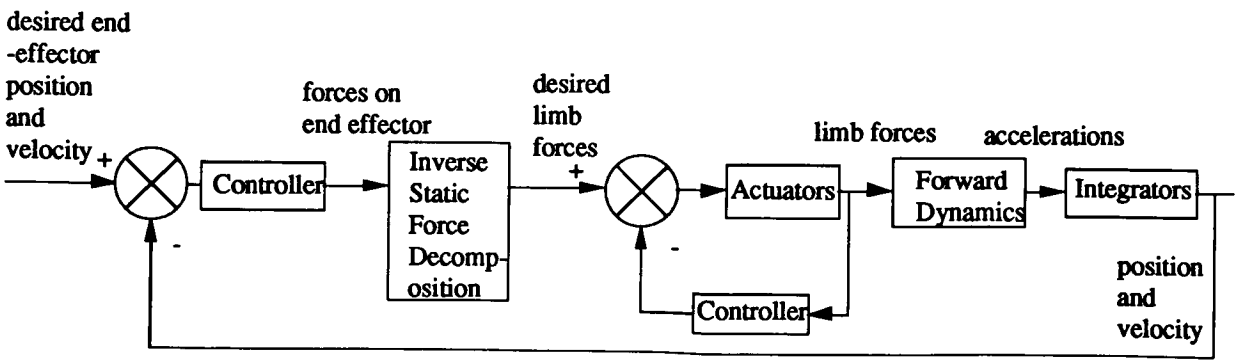

Figure 3. Block Diagram for Force Based Control Scheme.

The block diagram for the rate based control scheme is shown in Figure 2. In this control scheme, the hydraulic cylinders were controlled by dual stage servovalves. Within the servovalve, the spool position is fed back to the electromagnet with a spring. The block diagram for the servolvalve is given in Appendix B. The error in the position and the velocity are fed back to the current in the servovalve. The current in the servovalve is given by:

$$\mathbf{i} = -\mathbf{k_p I e_L} - \mathbf{k_v I \dot{e}_L} \tag{9}$$

where
$\mathbf{i}$ = 6×1 vector.
$\mathbf{k_p}$, $\mathbf{k_v}$ = constants.
$\mathbf{I}$ = 6×6 identity matrix.
$\mathbf{e_L}$ = error in limb lengths.
$\dot{\mathbf{e}}_L$ = error in limb length rates.

A decoupled controller with constant gains is chosen for the controller because the gains are associated with the hydraulic cylinders. Since all the hydraulic cylinders are identical, the gains are kept the same for all the cylinders.

The block diagram for the force based control scheme is shown in Fig. 3. In this control scheme, the cylinder were controlled by a proportional servovalve. It was found that the spool position feedback in the dual stage servovalve inhibited the response of the mechanism. The maximum spool opening from the servovalve was the same in both the valves to ensure that a fair comparison could be made in both the schemes.

The desired force in each of the limbs is given by:

$$\mathbf{F} = -\mathbf{H}^{-1}\left(\mathbf{K_p}\begin{bmatrix}\mathbf{e_p}\\ \mathbf{e_\theta}\end{bmatrix} + \mathbf{K_v}\begin{bmatrix}\dot{\mathbf{e}}_p\\ \dot{\mathbf{e}}_\theta\end{bmatrix}\right) \tag{10}$$

where
$\mathbf{K_p}$, $\mathbf{K_v}$ = Diagonal constant matrices.
$\mathbf{e_p}$ = error in position.
$\dot{\mathbf{e}}_p$ = error in velocity
$\mathbf{e_\theta}$ = error in angular position.
$\dot{\mathbf{e}}_\theta$ = error in angular velocity.

The gain matrices $\mathbf{K_p}$ and $\mathbf{K_v}$ are chosen to be diagonal matrices. At the current location of the end-effector, the off diagonal terms could have been chosen to decouple the system. This decoupling however, would not be possible for the complete workspace due to the change in the inertia matrix.

The error in the desired force in the limbs given by equation (10) and the actual force in the cylinder is fed back to the spool. The position of the spool is then given by:

$$\mathbf{X_s} = \mathbf{k_f e_f} \tag{11}$$

where
$\mathbf{k_f}$ = constant.
$\mathbf{e_f}$ = 6×1 error vector in the forces.

The gain for the force controller are kept the same for all the cylinders, since the cylinders are identical.

Rigid Body Dynamic Model

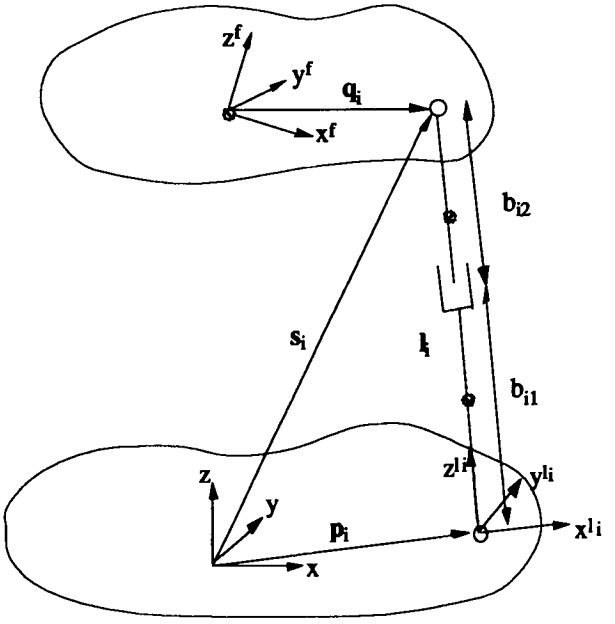

Figure 4. Parallel mechanism with a single limb and the variables.

The six degree of freedom parallel mechanism shown in Figure 1 consists of 13 rigid body elements. The six equations of motion can be obtained for each element, resulting in a large matrix (in this case 78×78 matrix) equation. This equation will be computationally expensive to solve. In the following section, a compact 6×6 matrix equation for the dynamics of the parallel mechanism is obtained. This would result in substantial savings in the computational time for the simulation.

The convention followed in the rest of the paper is as follows. All vectors and matrices are in bold letters. The superscript on the top left hand corner of a vector denotes the coordinate system. A superscript "t" refers to the fixed coordinate system coincident with the coordinate system attached to the top member and

"l_i" refers to the fixed coordinate system coincident to the coordinate system attached to the ith limb. No superscript signifies the fixed world coordinate system attached to the base member.

The equations of motion of the top member are given by:

$$\mathbf{M}^t\mathbf{a} = -\sum_i {}^t\mathbf{F}_{i3} + \mathbf{M}^t\mathbf{g}$$

$$\mathbf{J}^t\alpha = -\sum_i \left({}^t\mathbf{q}_i \times {}^t\mathbf{F}_{i3} + {}^t\mathbf{T}_{i3}\right) + {}^t\omega \times \mathbf{J}^t\omega \qquad (12)$$

where

$$\mathbf{M} = \begin{bmatrix} m & 0 & 0 \\ 0 & m & 0 \\ 0 & 0 & m \end{bmatrix}$$

$$\mathbf{J} = \begin{bmatrix} J_x & -J_{xy} & -J_{xz} \\ -J_{xy} & J_y & -J_{yz} \\ -J_{xz} & -J_{yz} & J_z \end{bmatrix}$$

${}^t\mathbf{g} = {}^t\mathbf{R}_b [0 \quad 0 \quad -g]^T$

g = acceleration due to gravity.

${}^t\mathbf{F}_{i3}$ = force applied by the top member to the ith limb.

${}^t\mathbf{T}_{i3}$ = Torque applied by top member to the ith limb.

${}^t\mathbf{q}_i$ = position of the ith force.

${}^t\omega$ = angular velocity of the top member in the top coordinate frame.

In the above equations, the forces are unknown. These forces are applied to the top member by the limbs. The additional equations will come from the dynamic analysis of the limbs. These dynamic equations will be in the form:

$${}^{l_i}\mathbf{a}_{i3} = \mathbf{D}_i {}^{l_i}\mathbf{F}_{i3} + \mathbf{d}_i \qquad (13)$$

where

$\mathbf{a}_{i3}$ = acceleration of the ith universal joint.

$\mathbf{F}_{i3}$ = force transmitted across the ith universal joint.

The development of the above equations for the parallel mechanism under consideration here are given in Appendix A.

The acceleration of the joint and the center of mass of the top member are related by:

$${}^{l_i}\mathbf{a}_{i3} = {}^{l_i}\mathbf{R}_t \left({}^t\mathbf{a} - \mathbf{qX}\,{}^t\alpha + \mathbf{t}\right) \qquad (14)$$

where

$$\mathbf{qX} = \begin{bmatrix} 0 & -{}^tq_{iz} & {}^tq_{iy} \\ {}^tq_{iz} & 0 & -{}^tq_{ix} \\ -{}^tq_{ix} & {}^tq_{ix} & 0 \end{bmatrix}$$

$$\mathbf{t} = \begin{bmatrix} -{}^tq_{ix}\left({}^t\omega_y^2 + {}^t\omega_z^2\right) + {}^t\omega_x\left({}^t\omega_z\,{}^tq_z + {}^t\omega_y\,{}^tq_y\right) \\ -{}^tq_{iy}\left({}^t\omega_z^2 + {}^t\omega_x^2\right) + {}^t\omega_y\left({}^t\omega_x\,{}^tq_x + {}^t\omega_z\,{}^tq_z\right) \\ -{}^tq_{iz}\left({}^t\omega_x^2 + {}^t\omega_y^2\right) + {}^t\omega_z\left({}^t\omega_y\,{}^tq_y + {}^t\omega_x\,{}^tq_x\right) \end{bmatrix}$$

Combining (13) and (14) and rearranging terms:

$$\begin{bmatrix} \mathbf{I}_{3\times3} & -\mathbf{qX} \end{bmatrix} \begin{bmatrix} {}^t\mathbf{a} \\ {}^t\alpha \end{bmatrix} = {}^t\mathbf{R}_{l_i} \mathbf{D}^{l_i}\mathbf{R}_t\, {}^t\mathbf{F}_{i3} + {}^t\mathbf{R}_{l_i}\mathbf{d}_i - \mathbf{t} \qquad (15)$$

The above constraint equation can be obtained for each limb. This will give 6 such equations.

Another set of constraint equations can be obtained for $\mathbf{T}_{i3}$. The angular accelerations of the upper part of the limb and the top member are related by:

$$\begin{bmatrix} - \\ - \\ {}^{l_i}\alpha_{iz} \end{bmatrix} = {}^{l_i}\mathbf{R}_t \begin{bmatrix} {}^t\alpha_x \\ {}^t\alpha_y \\ {}^t\alpha_z \end{bmatrix} \qquad (16)$$

The top two members of the above vector equation are not important and thus are left blank. This equation can be combined with the last equation in equation set (16) to get:

$${}^t\mathbf{T}_{i3} = -{}^t\mathbf{R}_{l_i} \begin{bmatrix} 0 & 0 & 0 \\ 0 & 0 & 0 \\ 0 & 0 & J_{i2z} \end{bmatrix} {}^{l_i}\mathbf{R}_t\, {}^t\alpha \qquad (17)$$

The equation of motion of the top member under the influence of forces $\mathbf{F}_{i3}$ are given by (12). Equation (15) can be used to eliminate forces $\mathbf{F}_{i3}$ from equation (12) and equation (17) can be used to eliminate $\mathbf{T}_{i3}$ from equation (2). This leads to:

$$\begin{bmatrix} \mathbf{M} + \sum_{i=1,6} {}^{t}\mathbf{R}_{l_i}\mathbf{D}_i^{-1}{}^{l_i}\mathbf{R}_t & \sum_{i=1,6} q\mathbf{X}^{t}\mathbf{R}_{l_i}\mathbf{D}_i^{-1}{}^{l_i}\mathbf{R}_t \\ \sum_{i=1,6} q\mathbf{X}^{t}\mathbf{R}_{l_i}\mathbf{D}_i^{-1}{}^{l_i}\mathbf{R}_t & \mathbf{J} + \sum_{i=1,6}\left({}^{t}\mathbf{R}_{l_i}\mathbf{J}_{i2z}{}^{l_i}\mathbf{R}_t - q\mathbf{X}^{t}\mathbf{R}_{l_i}\mathbf{D}_i^{-1}{}^{l_i}\mathbf{R}_t q\mathbf{X}\right) \end{bmatrix} \begin{bmatrix} {}^{t}\mathbf{a} \\ {}^{t}\alpha \end{bmatrix} = \begin{bmatrix} \sum_{i=1,6}\left({}^{t}\mathbf{R}_{l_i}\mathbf{D}_i^{-1}\mathbf{d}_i - {}^{t}\mathbf{R}_{l_i}\mathbf{D}_i^{-1}{}^{l_i}\mathbf{R}_t t\right) + \mathbf{M}^{t}\mathbf{g} \\ \sum_{i=1,6}\left(q\mathbf{X}^{t}\mathbf{R}_{l_i}\mathbf{D}_i^{-1}\mathbf{d} - q\mathbf{X}^{t}\mathbf{R}_{l_i}\mathbf{D}_i^{-1}{}^{l_i}\mathbf{R}_t t\right) + {}^{t}\omega \times \mathbf{J}^{t}\omega \end{bmatrix} \tag{18}$$

These equations can be used to solve for the accelerations of the top member. These are a very efficient form of the dynamic equations.

The above accelerations are in the coordinate system fixed to the top member. They can be transformed to the accelerations in the fixed coordinate frame by a simple coordinate transformation. Integrating the accelerations will give the velocity of the top member. The angular velocity of the top member can be used to calculate the euler angle rates using the following equation:

$$\begin{bmatrix} \dot{\alpha} \\ \dot{\beta} \\ \dot{\gamma} \end{bmatrix} = \mathrm{Sec}\beta \begin{bmatrix} \mathrm{Cos}\gamma & \mathrm{Sin}\gamma & 0 \\ -\mathrm{Sin}\gamma\,\mathrm{Cos}\beta & \mathrm{Cos}\gamma\,\mathrm{Cos}\beta & 0 \\ \mathrm{Cos}\gamma\,\mathrm{Sin}\beta & \mathrm{Sin}\gamma\,\mathrm{Sin}\beta & \mathrm{Cos}\beta \end{bmatrix} {}^{t}\omega \tag{19}$$

The above rigid body model was combined with the dynamic models for the hydraulic cylinder and the servolvalves. The details of these models are given in Appendix B.

Discussion of Results

The results from the simulation are shown in Figures (5)-(10). The top member was moved along the z-axis from a initial position of (0,0,140.0) to a final position of (0,0,140.2). while keeping the orientation fixed. The move was commanded at 0.1s from the start of the simulation to allow for the system to attain equilibrium. The gains for the controller were obtained by modifying the gains obtained from a linearized analysis.

The results from the rate based scheme are shown in Figures (5)-(7). The final position is obtained in 0.122s. The move in the z-direction induces oscillation in the x and y directions. If the gains are increased any further, the system will become unstable.

The results from the force based scheme are shown in Figures (8)-(10). The final z-position is reached in 0.058s. This is a 53% improvement in the step response of the mechanism in the z-direction. The gains in this system can be individually adjusted for each direction and thus the response in the x, y and z direction can be individually tailored. There is also a significant steady state error in the response. This is an expected error due to the weight of the top member and the upper part of the limbs. This error can be removed by adding a feedforward term to the controller. The mechanism in the beginning of the move can estimate the weight of the top member and then use this information in the feedforward term.

Conclusions

A simple constant gain force control scheme has been devised for the parallel mechanisms. This scheme is easy to implement and is better suited to parallel mechanisms than rate control schemes. The force control scheme requires the computation of $\mathbf{H}^{-1}$ while the rate control scheme uses the inverse position kinematics. The **H** matrix can be inverted symbolically to save on computational expense.

The preliminary results indicate that the force based control scheme will improve the response over the rate based control scheme. Further work, however is required to reach any comprehensive conclusions. There are important unanswered questions about the effect of the position of the end-effector and the payload mass on the response of the mechanism.

This control scheme can be easily adapted to control forces on the end effector. This capability will be crucial in applications of parallel mechanisms such as assembly tasks or partial/zero gravity simulators. The force control capabilities of the above control scheme also needs further investigation.

Acknowledgments

The author wishes to acknowledge the support of NASA JSC grant no NAG 9-672 for the above research.

References

[1] D'Azzo, J. J., and Houpis, C. H., "Linear Control System Analysis and Design", McGraw Hill Book Co., 1988.

[2] Featherstone, R., "Robot Dynamics Algorithms", Kluwer Academic Publishers, 1987.

[3] Fichter, E. F., "A Stewart Platform - Based Manipulator: General Theory and Practical Construction", International Journal of Robotics Research, vol. 5, No. 2, pp. 157-182, Summer 1986.

[4] Hunt, K. H., "Structural Kinematics of In-Parallel-Actuated Robot-Arms", Trans. ASME J. of Mechanisms, Transmissions, and Automation in Design, Vol 105, pp. 705-712, 1983.

[5] Lee, K. M., and Shah, D. K., "Kinematic Analysis of a Three Degree of Freedom In - Parallel Actuated Manipulator", Proceedings of the 1987 IEEE International Conference on Robotics and Automation, vol. 1, pp 345-350, 1987.

[6] McCallion, H., and Truong, P. D., "The analysis of a Six-Degree-of-Freedom Work Station for Mechanized Assembly", Proceedings of Fifth World Congress for the Theory of Machines and Mechanisms, ASME, pp. 611-616, 1979.

[7] Merlet, J. P., "Parallel Manipulators", Seventh CISM-IFToMM Symposium on theory and practice of Robots and Manipulators, pp. 317-324, Sept. 1988.

[8] Moog, "Type 30 Flow Control Servovalves", Catalog 301 385, Moog Inc.

[9] Nanua, P., and Waldron, K. J., "Direct Kinematic Solution of a Special Parallel Robot Structure", Proceedings of CISM-IFToMM Symposium on Theory and Practice of Robots and Manipulators, Cracow, Poland, 1990.

[10] Nanua, P., Waldron, K. J., and Murthy, V., "Direct Kinematic Solution of a Stewart Platform", IEEE Transactions on Robotics and Automation, August 1990.

[11] Potton, S. L., "GEC Advanced Device for Assembly", Proceedings of the CIRP Conference on Assembly and Automation, pp. 126-128, June 1983.

[12] Stewart, D., "A Platform with Six Degrees of Freedom", Proc. Inst. Mech. Engr, 180(1):371-386, 1965.

[13] Sugimoto, K., "Kinematic & Dynamic Analysis of Parallel Manipulators by Means of Motor Algebra," Trans. ASME J. of Mechanisms, Transmissions, and Automation in Design, vol. 109, pp. 3-7, 1987.

[14] Waldron, K. J., and Hunt, K. H., "Series - Parallel Dualities in Actively Coordinated Mechanisms", 4th Int. Symposium on Robotics Research, Santa Cruz, CA, 1987.

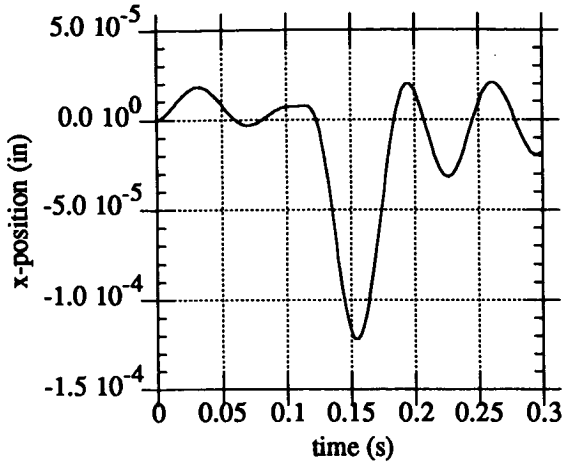

Figure 5. X-Position under rate-based control scheme.

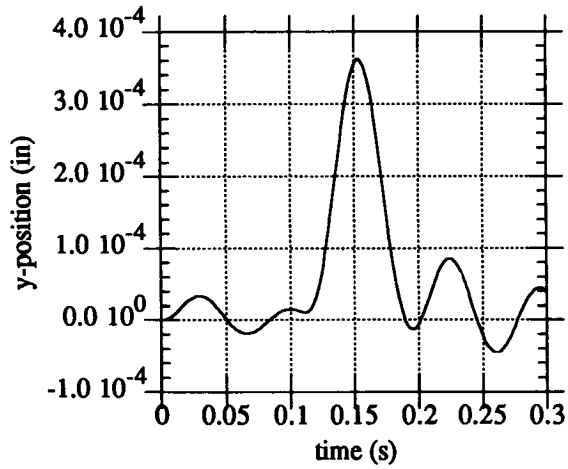

Figure 6. Y-Position under rate-based control scheme.

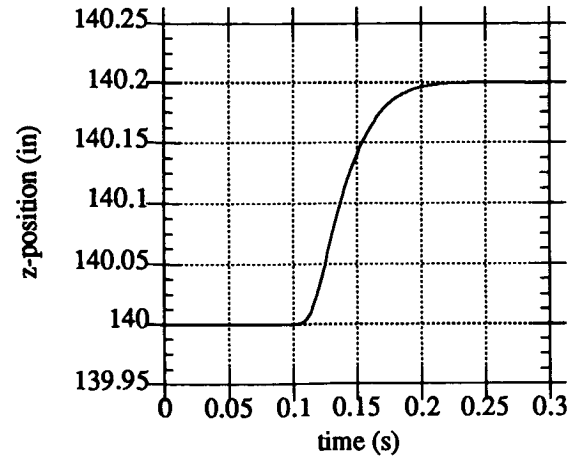

Figure 7. Z-Position under rate-based control scheme.

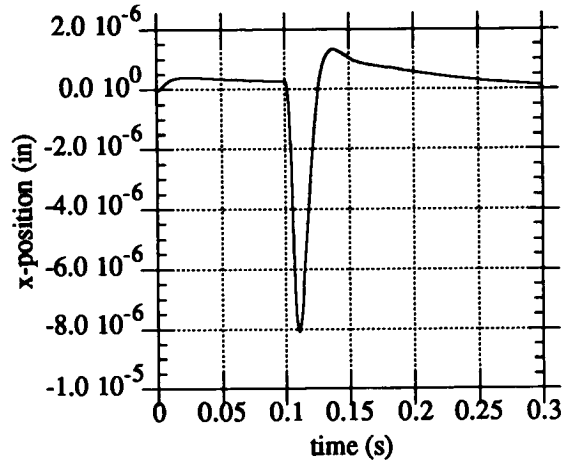

Figure 8. X-Position for force-based control scheme.

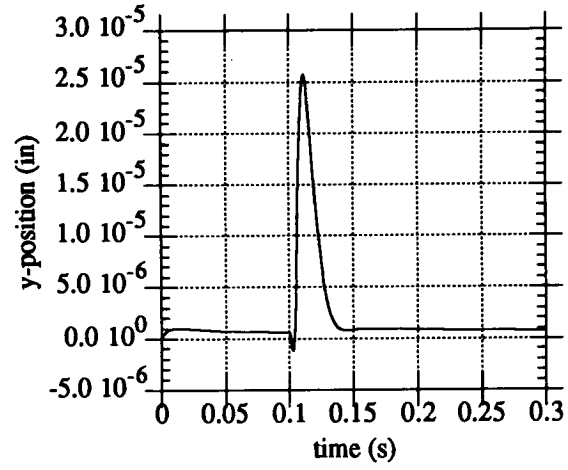

Figure 9. Y-Position for force-based control scheme.

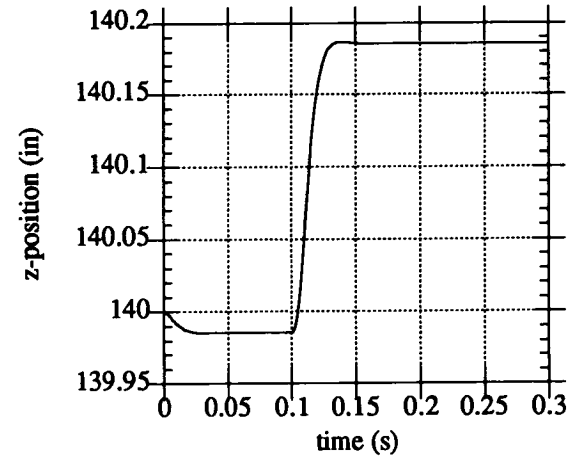

Figure 10. Z-Position for force-based control scheme.

Appendix A

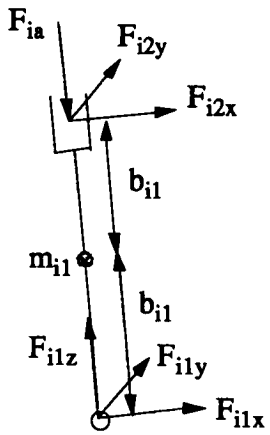

Figure a1. Free body diagram of the lower part of limb.

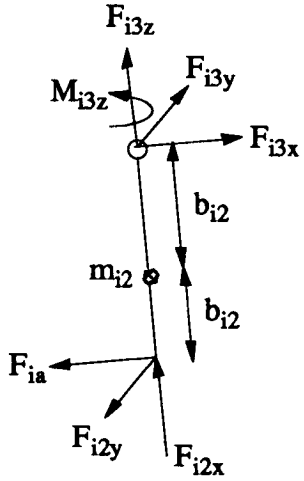

Figure a2. Free body diagram of the upper part of the limb.

Given the position of the coordinate system attached to the top member and its orientation, the position vector of the ith joint on the top member, in the fixed coordinate system can be computed by

$$\mathbf{s_i} = {}^{b}\mathbf{R}_t \, {}^{t}\mathbf{q_i} + \mathbf{r}$$

where

$$ {}^{b}\mathbf{R}_t = \begin{bmatrix} \text{Cos}\gamma\,\text{Cos}\beta & -\text{Sin}\gamma\,\text{Cos}\alpha + \text{Cos}\gamma\,\text{Sin}\beta\,\text{Sin}\alpha & \text{Sin}\gamma\,\text{Sin}\alpha + \text{Cos}\gamma\,\text{Sin}\beta\,\text{Cos}\alpha \\ \text{Sin}\gamma\,\text{Cos}\beta & \text{Cos}\gamma\,\text{Cos}\alpha + \text{Sin}\gamma\,\text{Sin}\beta\,\text{Sin}\alpha & -\text{Cos}\gamma\,\text{Sin}\alpha + \text{Sin}\gamma\,\text{Sin}\beta\,\text{Cos}\alpha \\ -\text{Sin}\beta & \text{Cos}\beta\,\text{Sin}\alpha & \text{Cos}\beta\,\text{Cos}\alpha \end{bmatrix} $$

${}^{t}\mathbf{q_i}$ = position of ith joint in the top coordinate system.

$\mathbf{r}$ = position of the origin of the top coordinate system in the fixed coordinate system.

The vectors along the limbs in the fixed coordinate system are given by:

$$\mathbf{l_i} = \mathbf{s_i} - \mathbf{p_i}$$

The limb lengths are the magnitude of this vector:

$$l_i = \frac{\mathbf{l_i}}{|\mathbf{l_i}|}$$

For each limb, a coordinate system attached to the limb is setup. The limbs will be assumed to be axisymmetric. The z-axis for the new limb coordinate system is along the limb. The x-axis is perpendicular to the z-axis of the limb coordinate system and the x-axis of the fixed coordinate system. Thus the rotation matrix is given by:

$$ {}^{b}\mathbf{R}_{l_i} = \begin{bmatrix} \sqrt{1-l_{ix}^2} & 0 & l_{ix} \\ -\dfrac{l_{ix}l_{iy}}{\sqrt{1-l_{ix}^2}} & \dfrac{l_{iz}}{\sqrt{1-l_{ix}^2}} & l_{iy} \\ -\dfrac{l_{ix}l_{iz}}{\sqrt{1-l_{ix}^2}} & -\dfrac{l_{iy}}{\sqrt{1-l_{ix}^2}} & l_{iz} \end{bmatrix} $$

where

l_{ix}, l_{iy}, l_{iz} = components of the vector $\mathbf{l_i}$.

The velocity of the ith joint is given by:

$$ {}^{t}\dot{\mathbf{s}}_i = {}^{t}\mathbf{v} + {}^{t}\boldsymbol{\omega} \times {}^{t}\mathbf{q_i} $$

where

${}^{t}\mathbf{v}$ = velocity of the center of mass (coincident with the origin) of the top member.

${}^{t}\boldsymbol{\omega}$ = angular velocity of the center of mass of the top member.

The velocity of the ith joint in the limb coordinate system is:

$$ {}^{l_i}\dot{\mathbf{s}}_i = {}^{l_i}\mathbf{R}_t \, {}^{t}\dot{\mathbf{s}}_i $$

where

$ {}^{l_i}\mathbf{R}_t = {}^{l_i}\mathbf{R}_b \, {}^{b}\mathbf{R}_t $

In the following section, all the variables are in the limb coordinate system. The superscript is avoided for clarity.

The angular velocity of the ith limb in the limb coordinate system is given by:

$$\omega_{ix} = -\frac{\dot{s}_{iy}}{l}$$

$$\omega_{iy} = -\frac{\dot{s}_{ix}}{l}$$

The velocity of the prismatic joint is given by:

$$\dot{l} = \dot{s}_{iz}$$

The required equations of motion of the bottom link are:

$$T_{i2x} = \left(J_{i1x} + m_{i1}b_{i11}^2\right)\alpha_{ix} + b_{i1}F_{i2y} + b_{i11}m_{i1}g_{iy}$$

$$T_{i2y} = \left(J_{i1y} + m_{i1}b_{i11}^2\right)\alpha_{iy} + b_{i1}F_{i2x} + b_{i11}m_{i1}g_{ix} \quad (a1)$$

where

J_{i1x} = mass moment of inertia of the lower limb about the x-axis.

J_{i1y} = mass moment of inertia of the lower limb about the y-axis.

$\begin{bmatrix} g_{ix} \\ g_{iy} \\ g_{iz} \end{bmatrix} = {}^{l_i}\mathbf{R}_b \begin{bmatrix} 0 \\ 0 \\ -g \end{bmatrix}$ = gravity vector in the limb coordinate system.

g = acceleration due to gravity (9.81 m/s^2).

The equation of motion of the top limb are given by:

$$m_{i2}\left[(l_i - b_{i22})\alpha_{iy} + 2\dot{l}_i\omega_{iy}\right] = F_{i3x} - F_{i2x} + m_{i2}g_{ix}$$

$$m_{i2}\left[-(l_i - b_{i22})\alpha_{ix} - 2\dot{l}_i\omega_{ix}\right] = F_{i3y} - F_{i2y}$$

$$+m_{i2}g_{iy}$$

$$m_{i2}\left[\ddot{l}_i - (l_i - b_{i22})\left(\omega_{ix}^2 + \omega_{iy}^2\right)\right] = F_{i3z} - F_{i2z}$$

$$+m_{i2}g_{iz}$$

$$J_{i2x}\alpha_{ix} = -b_{i22}F_{i3y} - b_{i21}F_{i2y} - T_{i2x}$$

$$J_{i2y}\alpha_{iy} = b_{i22}F_{i3x} + b_{i21}F_{i2x} - T_{i2y}$$

$$J_{i2z}\alpha_{iz} = T_{i3x} \quad (a2)$$

where

$\alpha_{ix}, \alpha_{iy}, \alpha_{iz}$ = angular acceleration of the limb in the limb coordinate system.

m_{i2} = mass of the upper part of ith limb.

$J_{i2x}, J_{i2y}, J_{i2z}$ = mass moment of inertia of the upper part of ith limb about its center of mass.

Combining equations (a1) and (a2):

$$\alpha_{iy} = c_{i11}F_{i3x} + c_{i12}$$

$$\alpha_{ix} = c_{i21}F_{i3y} + c_{i22}$$

$$\ddot{l}_i = c_{i31}F_{i3x} + c_{i32} \quad (a3)$$

where

$$c_{i11} = \frac{l_i}{J_{i1y} + J_{i2y} + m_{i1}b_{i11}^2 + m_{i2}(l_i - b_{i22})^2}$$

$$c_{i21} = -\frac{l_i}{J_{i1x} + J_{i2x} + m_{i1}b_{i11}^2 + m_{i2}(l_i - b_{i22})^2}$$

$$c_{i12} = \frac{\left[m_{i1}b_{i11} + m_{i2}(l_i - b_{i22})\right]g_{ix}}{J_{i1y} + J_{i2y} + m_{i1}b_{i11}^2 + m_{i2}(l_i - b_{i22})^2}$$

$$-\frac{2m_{i2}\dot{l}_i\omega_{iy}(l_i - b_{i22})}{J_{i1y} + J_{i2y} + m_{i1}b_{i11}^2 + m_{i2}(l_i - b_{i22})^2}$$

$$c_{i22} = -\frac{\left[m_{i1}b_{i11} + m_{i2}(l_i - b_{i22})\right]g_{iy}}{J_{i1x} + J_{i2x} + m_{i1}b_{i11}^2 + m_{i2}(l_i - b_{i22})^2}$$

$$-\frac{2m_{i2}\dot{l}_i\omega_{ix}(l_i - b_{i22})}{J_{i1x} + J_{i2x} + m_{i1}b_{i11}^2 + m_{i2}(l_i - b_{i22})^2}$$

$$c_{i31} = \frac{1}{m_{i2}}$$

$$c_{i32} = \frac{F_{ia} + m_{i2}g_{iz} + m_{i2}(l_i - b_{i22})\left(\omega_{ix}^2 + \omega_{iy}^2\right)}{m_{i2}}$$

F_{ia} = force from the actuator

The angular acceleration in equation (a3) are related to the acceleration of the top joint by the equation:

$$\alpha_{ix} = \frac{-a_{i3y} - 2\dot{l}_i\omega_{ix}}{l_i}$$

$$\alpha_{iy} = \frac{a_{i3x} - 2\dot{l}_i\omega_{iy}}{l_i} \quad (a4)$$

Combining equations (a3) and (a4):

$$\mathbf{a}_{i3} = \mathbf{D}_i\mathbf{F}_{i3} + \mathbf{d}_i \quad (a5)$$

where

$$\mathbf{a}_{i3} = \begin{bmatrix} a_{i3x} & a_{i3y} & a_{i3z} \end{bmatrix}^T$$

$$\mathbf{F}_{i3} = \begin{bmatrix} F_{i3x} & F_{i3y} & F_{i3z} \end{bmatrix}^T$$

$$\mathbf{D}_i = \begin{bmatrix} c_{i11}l_i & 0 & 0 \\ 0 & -c_{i21}l_i & 0 \\ 0 & 0 & c_{i31} \end{bmatrix}$$

$$\mathbf{d}_i = \begin{bmatrix} c_{i12} l_i + 2\dot{i}\omega_{iy} \\ -c_{i22} l_i - 2\dot{i}\omega_{ix} \\ c_{i32} - l\left(\omega_{ix}^2 + \omega_{iy}^2\right) \end{bmatrix}$$

This matrices $\mathbf{D}_i$ and $\mathbf{d}_i$ in this equation can be computed for each limb.

Appendix B

The model for the two stage servovalves for small displacements is given by the block diagram in Fig. 1.

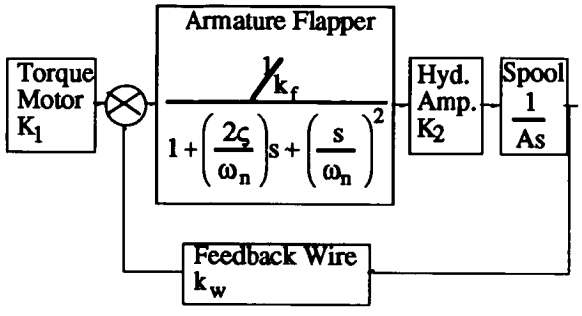

Figure b1. Block Diagram of Flow Control hydraulic servovalve ([8]).

The flow through an orifice is given by the equation:

$$Q = KA\sqrt{p_1 - p_2} \tag{b1}$$

where
Q = volume flow rate.
A = area of the orifice.
p_1 = pressure on one side of the orifice.
p_2 = pressure on the other side of the orifice.
K = constant.

For a positive displacement of the servovalve x_S, the supply pressure is connected to chamber 2 of the cylinder and the return side is connected to the chamber 1. The equations are given by:

$$Q_{in} = K_s x_s \sqrt{p_s - p_2} + K_l(p_1 - p_2) \tag{b2}$$

$$Q_{out} = K_s x_s \sqrt{p_1 - p_r} - K_l(p_1 - p_2) \tag{b3}$$

These flow rates are equal to the corresponding volume changes in the chambers. These change are given by:

$$Q_{in} = \dot{i}A_2 + \frac{A_2(1 - b_2)}{\beta}\frac{dp_2}{dt} \tag{b4}$$

$$Q_{out} = \dot{i}A_1 - \frac{A_1(b_1 + b_2 - 1)}{\beta}\frac{dp_1}{dt} \tag{b5}$$

Using the above set of equations:

$$\frac{A_2(1 - b_2)}{\beta}\frac{dp_2}{dt} = K_s|x_s|\sqrt{p_s - p_2} - \dot{i}A_2 + K_l(p_1 - p_2) \tag{b6}$$

$$\frac{A_1(b_1 + b_2 - 1)}{\beta}\frac{dp_1}{dt} = -K_s|x_s|\sqrt{p_1 - p_r} + \dot{i}A_1 - K_l(p_1 - p_2) \tag{b7}$$

If x_S is negative, then these equations are:

$$\frac{A_2(1 - b_2)}{\beta}\frac{dp_2}{dt} = -K_s|x_s|\sqrt{p_2 - p_r} - \dot{i}A_2 + K_l(p_1 - p_2) \tag{b8}$$

$$\frac{A_1(b_1 + b_2 - 1)}{\beta}\frac{dp_1}{dt} = K_s|x_s|\sqrt{p_s - p_1} + \dot{i}A_1 - K_l(p_1 - p_2) \tag{b9}$$

The above set of differential equations can be solved to obtain the pressure in the cylinder chambers. The force on the limb is given by:

$$F_{ia} = p_2 A_2 - p_1 A_1 - c\dot{i} \tag{b10}$$

where
c = damping coefficient.

This completes the development of the equations for the hydraulic cylinder.